Removal of Fe(III) from ethanol by silica-gel supported ester-terminated PAMAM dendrimers: experimental and DFT calculation

Shuqin Zhang, Yuzhong Niu*, Zhenchi Chen, Hou Chen, Zhenglong Yang, Liangjiu Bai, Baiqing Yuan

School of Chemistry and Materials Science, Ludong University, Yantai 264025, China, Tel. +86 535 6696162,
email: 1245788533@qq.com (S. Zhang), Tel. +86 535 6696162, Fax +86 535 6696162, email: niuyuzhong@ldu.edu.cn (Y. Niu),
Tel. +86 535 6696162, email: 1937455735@qq.com (Z. Chen), Tel. +86 535 6696162, email: chenhou@ldu.edu.cn (H. Chen),
Tel. +86 535 6696162, email: yzl@iccas.ac.cn (Z. Yang), Tel. +86 535 6696162, email: bailiangjiu@ldu.edu.cn (L. Bai),
Tel. +86 535 6696162, email: baiqingyuan1981@126.com (B. Yuan)

ABSTRACT

Silica-gel supported ester-terminated polyamidoamine (PAMAM) dendrimers (SG-G0.5, SG-G1.5, and SG-G2.5) were utilized as adsorbents for the removal of Fe(III) from fuel ethanol. The adsorption property was systematically investigated by determining the effects of dendrimer generation, contact time, temperature, initial Fe(III) concentration, and adsorbent dosage on the adsorption. Static saturated adsorption indicates the adsorption capacity increases with the increasing of dendrimer generation by following the sequence of SG-G2.5 > SG-G1.5 > SG-G0.5. Adsorption kinetic shows that the adsorption equilibrium can reach within 200 min for all the adsorbents. The adsorption kinetic can be well fitted by pseudo-second-order model and is controlled by film diffusion process. Adsorption isotherm demonstrates the adsorption favors high temperature and initial Fe(III) concentration. The adsorption isotherm follows Langmuir model and carries out by monolayer chemical ion-exchange mechanism. Thermodynamic parameters imply the adsorption process of Fe(III) by SG-G0.5, SG-G1.5 and SG-G2.5 is a spontaneous, endothermic and entropy increased process. The regeneration property shows the adsorbents exhibit good reusability and maintain excellent adsorption capacity after three adsorption-desorption cycles. Fourier transform infrared spectroscopy (FTIR) and density functional theory (DFT) calculation indicate the interaction of carbonyl oxygen and amine nitrogen groups with Fe(III) mainly dominate the adsorption process.

Keywords: Adsorption; Silica-gel; PAMAM dendrimers; Fe(III); Ethanol

1. Introduction

With the development of modern industry and transportation, atmospheric pollution and energy crisis caused by fossil fuel consumption have posed serious threat to environmental safety and sustainable development [1,2]. Therefore, it is urgent and crucial to develop green and renewable energy to replace the nonrenewable fossil fuel. In recent years, numerous alternative energy sources such as hydrogen energy, biodiesel, and ethanol have captured more and more attentions due to their environment-friendly, renewable, and recyclable [3–6]. Among them, ethanol is widely used as substitution for gasoline and diesel due to the similarity in physical and chemical property [7]. Moreover, it can reduce the exhaust gas emission and can be acquired from wide range of sources such as corn, wheat, sugar cane, and other raw biomass materials [4,7].

However, metal ions would be inevitably introduced into ethanol during the production, fermentation, transportation and storage process [8–10]. The existence of metal ions not only decreases the quality of ethanol, but also brings adverse effect for its usage. For example, when etha-

*Corresponding author.

nol is used as fuel for automobile, the presence of metal ions would damage the engine, reduce the efficiency of engine and catalytic reactor of vehicle exhaust system [7,11]. Furthermore, metal ions would be released to the environment along with the exhaust gases, which could cause destructive effect to ecological safety due to its high toxic and non-biodegradable [12,13]. Thus, it is of vital importance to remove metal ions from ethanol.

A number of approaches have been explored for the removal of metal ions from aqueous and ethanol solution, such as membrane filtration, chemical precipitation, electrolysis, ion exchange, solvent extraction, and adsorption [7,12,14]. Compared with other technologies, adsorption is preferred due to its cost-effectiveness, high efficiency, and simple operation [7,13]. Diverse adsorbents including chitosan [15], activated carbon [16], graphene oxide [17], zeolite[18] and silica-gel [19] have been constructed for the decontamination of metal ions. Compared with other adsorbents, silica-gel based adsorbents have attract considerable interests due to the inherent advantages of porous structure, large surface area, good thermal and mechanical stability, and feasible functionalized surface property [19–21]. Different functional groups have been employed to modified silica-gel to enhance its adsorption performance [22,23]. PAMAM dendrimer which contains plenty of nitrogen and oxygen atoms exhibits excellent binding ability for metal ions [24–26]. Hence, the decoration of silica-gel with PAMAM dendrimer is an effective way to construct efficient adsorbent [27]. However, the majority of the reports relate with this series of adsorbents are mainly focus on the removal of metal ions from aqueous solution [19,25,28–30]. Qu et al. reported the pioneer work of removal Cu(II) from ethanol via silica-gel supported amino-terminated PAMAM dendrimers [31]. Subsequently, our group reported the adsorption of Co(II), Hg(II), and Ag(I) from ethanol by a series of silica-gel supported PAMAM dendrimers with different peripheral groups, and the results suggest that the adsorption behavior depends greatly on the dendrimer generation and terminal group [7,10].

In this study, the feasibility of silica-gel supported ester-terminated polyamidoamine (PAMAM) dendrimers (SG-G0.5, SG-G1.5, and SG-G2.5) for the removal of Fe(III) from ethanol was investigated systematically. The effects of dendrimer generation, contact time, temperature, initial

Fe(III) concentration, and adsorbent dosage on the adsorption were determined. The adsorption mechanism was revealed based on the results of experiment and density functional theory (DFT) calculation.

2. Experimental

2.1. Materials and methods

Silica-gel supported ester-terminated PAMAM dendrimers (SG-G0.5, SG-G1.5, and SG-G2.5) that illustrated in Fig. 1 were prepared by divergent method according to our previous research [7]. The stock solution of Fe(III) with $0.01 \ mol \cdot L^{-1}$ was prepared by dissolving $0.6758 \ g \ FeCl_3 \cdot 6H_2O$ in 250 mL anhydrous ethanol. The reagents used were all analytical grades and obtained from Sinopharm Chemical Reagent Co., Ltd (China). The concentration of Fe(III) was determined by a VARIAN AA240 atomic adsorption spectrophotometer (AAS). FTIR was recorded on a Nicolet iS50 (Thermo Fisher Scientific, USA). The DFT calculation was performed by using Gaussian 03 program [32].

2.2. Adsorption property for Fe(III)

The adsorption performance of SG-G0.5, SG-G1.5, and SG-G2.5 for Fe(III) from ethanol was evaluated by batch method. The experiment procedure of static saturated adsorption was as follows: 20 mL $0.001 \ mol \cdot L^{-1}$ Fe(III) solution and 25 mg adsorbent were added in the flask and shaken for 12 h at 25°C. After that, the concentration of Fe(III) was detected by AAS. The effects of the contact time, initial Fe(III) concentration, temperature and the adsorbent dosage on the adsorption were demonstrated according to the similar procedure described in previous reports and listed in detail in the supporting information [7]. The adsorption capacity and removal rate were calculated by Eqs. (1) and (2), respectively.

$$q = \frac{(C_o - c)V}{W} \tag{1}$$

$$Removal\ rate = \frac{C_0 - C}{C_0} \times 100\% \tag{2}$$
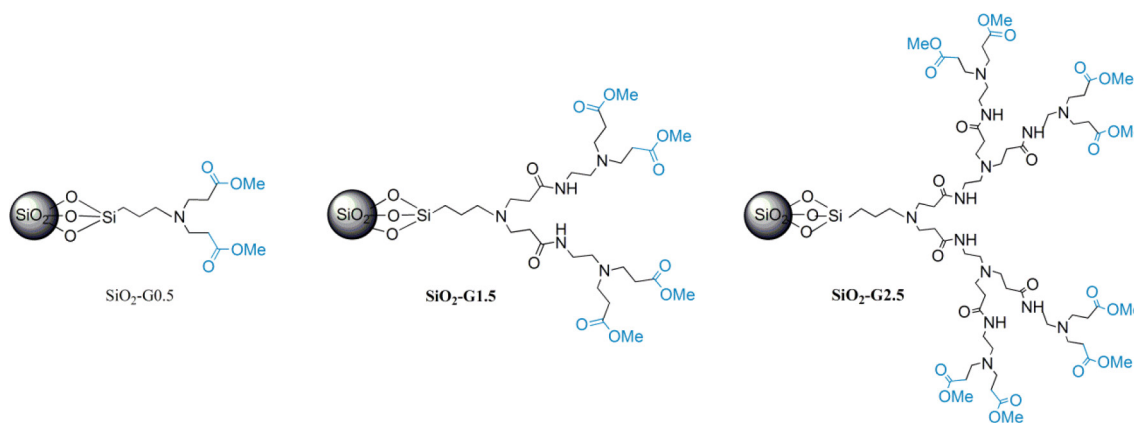

Fig. 1. Structure diagram of SG-G0.5, SG-G1.5, and SG-G2.5.

where q is the adsorption amount (mmol·g^{-1}); C_0 and C are the initial and equilibrium concentration of Fe(III) (mmol·mL^{-1}), respectively; V represents the volume (mL) and W denotes the weight of adsorbent (g).

2.3. Regeneration property

About 25 mg adsorbent that uptake Fe(III) was added to 20 mL 5% thiourea-0.5 mol·L^{-1} HNO$_3$ solution [33,34]. The mixture was shaken for 3 h and the concentration of Fe(III) was detected. The desorption rate was calculated as the ratio of desorbed amount to adsorbed amount.

2.4. Adsorption mechanism

The coordination mode and interaction mechanism of PAMAM dendrimer with Fe(III) was simulated by selecting G0.5 as model due to the symmetry structure of the dendrimer. The geometry optimization of the complexes that possible formed during the adsorption was performed using DFT method at B3LYP/6-31+G(d) (LANL2DZ for Fe(III)) level [7,35,36]. After that, the binding energy and the interaction mechanism were revealed based on natural bond orbital (NBO) analysis at the level of B3LYP/6-31+G(d) (LANL2DZ for Fe(III)) // B3LYP/6-311+G(d, p) (LANL2DZ for Fe(III)) [7]. The binding energy was calculated as the energy difference between the complex and that of G0.5 and Fe(III).

3. Results and discussion

3.1. Static saturated adsorption

The static saturated adsorption capacity of SG-G0.5, SG-G1.5, and SG-G2.5 for Fe(III) is shown in Fig. 2. It can be seen that the adsorption capacity for Fe(III) follows the sequence of SG-G2.5 > SG-G1.5 > SG-G0.5, indicating the adsorption capacity of silica-gel supported ester-terminated PAMAM dendrimer increases with the increase of dendrimer generation. The reason can be reasonable interpreted by the increase content of functional groups with the raising of dendrimer generation, which provides more active sites for the binding of Fe(III).
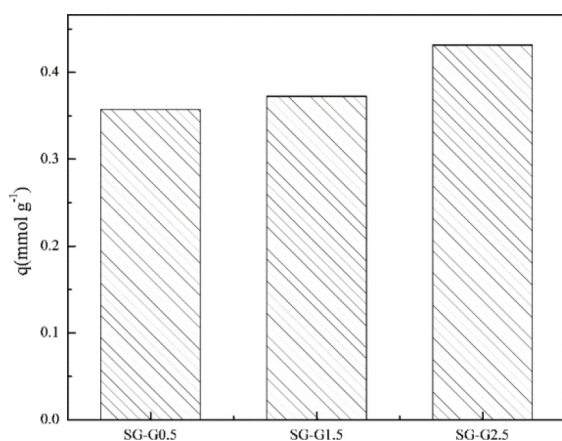
3.2. Adsorption kinetic

The adsorption kinetic profiles for Fe(III) are shown in Fig. 3. The adsorption of Fe(III) increases promptly within the first 90 min and then rises slowly until reaches equilibrium at about 200 min for the three adsorbents. At the beginning of the adsorption, there are plenty of active binding sites and the concentration of Fe(III) is high, which facilitate the diffusion and coordination of Fe(III) with the adsorbent, leading to the fast adsorption. With the proceeding of the adsorption, the active binding sites and the concentration of Fe(III) decrease accordingly, leading to the slowdown of the adsorption rate. Furthermore, the equilibrium adsorption capacity of the adsorbents follows the sequence of SG-G2.5 > SG-G1.5 > SG-G0.5, which is consistent with the results of static adsorption.

The pseudo-first-order kinetic model, pseudo-second-order kinetic model, and Boyd film diffusion model are often adopted to reveal the adsorption kinetic mechanism [37–42]. The detail description of these models is provided in the supporting information. The fitting parameters are summarized in Tables 1 and 2. It can be seen from Table 1, the regression coefficients of pseudo-second-order kinetic model (R_2^2) are higher than the corresponding pseudo-first-order kinetic model (R_1^2), and the calculated adsorption capacity ($q_{e,cal}$) obtained from pseudo-second-order kinetic model is more close to the experimental value. The results indicate the adsorption kinetic can be well depicted by pseudo-second-order kinetic model. The fitting plots of Bt versus t that shown in Table 2 exhibit excellent linearity and do not pass through the origin, suggesting the adsorption kinetic is controlled by film diffusion process.

3.3. Adsorption isotherm

The adsorption isotherm curves for Fe(III) are presented in Fig. 4. It is clear that the adsorption capacity increases with the increase of initial Fe(III) concentration due to the increasing possibility of Fe(III) to bind with the active sites at high concentration. Additionally, it also observed the adsorption favors high temperature, which indicates the endothermic nature of the adsorption.
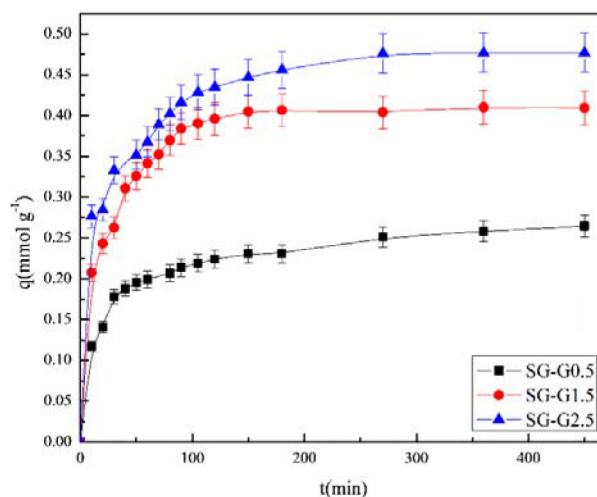

Fig. 2. Static saturated adsorption for Fe(III).

Fig. 3. Adsorption kinetic profiles for Fe(III).

Table 1
Adsorption kinetic parameters for Fe(III)

Adsorbent	$q_{e,exp}$ (mmol·g^{-1})	Pseudo-first-order kinetics			Pseudo-second-order kinetics		
		$q_{e,cal}$ (mmol ·g^{-1})	k_1 (min^{-1})	R_1^2	$q_{e,cal}$ (mmol·g^{-1})	k_2 (mmol·g^{-1}·min^{-1})	R_2^2
SG-G0.5	0.26	0.12	0.0081	0.9698	0.27	0.1658	0.9980
SG-G1.5	0.41	0.19	0.0184	0.8426	0.42	0.1944	0.9992
SG-G2.5	0.48	0.33	0.0192	0.9276	0.50	0.1227	0.9993

Table 2
The linear equations and corresponding parameters of B_t versus t plots

Adsorbent	Linear equation	Intercept error	R^2
SG-G0.5	$B_t = 0.0083t + 0.3305$	0.0476	0.9867
SG-G1.5	$B_t = 0.0268t - 0.1839$	0.0933	0.9794
SG-G2.5	$B_t = 0.0142t + 0.2269$	0.0293	0.9963

Langmuir, Freundlich, and Dubinin-Radushkevich (D-R) models are employed to analyze the isotherm data for the sake of the adsorption mechanism [43–47]. The linear equations of the models are provided in the supporting information, and the fitting parameters of three models are shown in Tables 3 and 4. According to Table 3, the Langmuir model is more reasonable to describe the adsorption isotherm of Fe(III) due to the higher regression coefficient of Langmuir model (R_L^2). In addition, the calculated adsorption capacity from Langmuir model is in agreement with the experimental value, further

demonstrating the valid of Langmuir model. It is found that the E values in Table 4 are all higher 8 KJ·mol^{-1}, illustrating the adsorption takes place by chemical ion-exchange mechanism.

3.4. Thermodynamics parameters

The thermodynamic parameters of Gibbs free energy change (ΔG), enthalpy (ΔH), and entropy (ΔS) for the adsorption are calculated according to Eqs. (3) and (4) [7,48]:

$$\Delta G = \Delta H - T\Delta S \tag{3}$$

$$InK_L = \frac{\Delta S}{R} - \frac{\Delta H}{RT} \tag{4}$$

where K_L represents the Langmuir constant, R is gas constant (8.314J·mol^{-1}·K^{-1}), and T is absolute temperature (K). The calculated results are summarized in Table 5, it can be seen that the values of ΔG are all negative, indi-
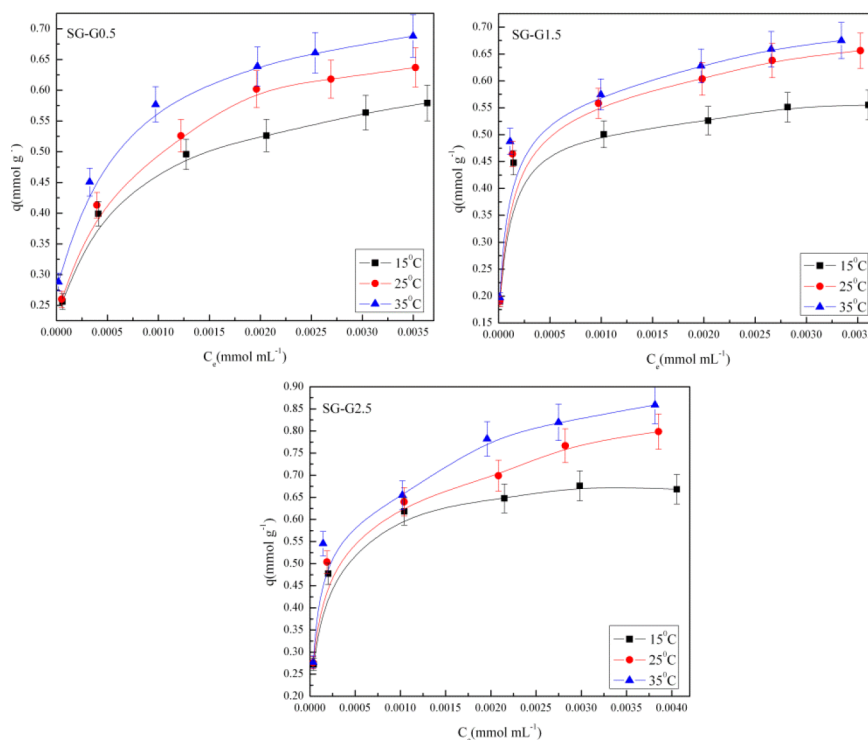

Fig. 4. Adsorption isotherm curves for Fe(III).

Table 3
Adsorption isotherm parameters for Fe(III)

Adsorbent	T (°C)	Langmuir			Freundlich		
		q_m (mmol·g^{-1})	K_L (mL·mmol^{-1})	R_L^2	K_F (mmol·g^{-1})	n	R_F^2
SG-G0.5	15	0.60	5412.03	0.9962	1.79	5.07	0.9911
	25	0.66	5029.03	0.9954	2.24	4.62	0.9945
	35	0.70	6933.89	0.9962	1.85	5.79	0.9955
SG-G1.5	15	0.56	15999.03	0.9968	1.60	5.75	0.8504
	25	0.66	10634.49	0.9967	2.21	4.92	0.8952
	35	0.68	11843.77	0.9986	2.20	5.08	0.8718
SG-G2.5	15	0.68	11640.90	0.9934	2.08	5.28	0.9013
	25	0.81	5921.71	0.9930	2.67	4.73	0.9481
	35	0.88	5911.82	0.9995	3.05	4.55	0.8981

Table 4
The fitting parameters of D-R isotherm model for Fe(III)

Adsorbent	T (°C)	Linear equation	q_m (mmol·g^{-1})	k (mol^2·J^{-2})	E (kJ·mol^{-1})	R^2
SG-G0.5	15	$y = -2.24 \cdot 10^{-9}x - 0.14$	0.87	$2.24 \cdot 10^{-9}$	14.94	0.9995
	25	$y = -2.26 \cdot 10^{-9}x$	1.00	$2.26 \cdot 10^{-9}$	14.88	0.9946
	35	$y = -1.58 \cdot 10^{-9}x - 0.06$	0.94	$1.58 \cdot 10^{-9}$	17.80	0.9859
SG-G1.5	15	$y = -1.83 \cdot 10^{-9}x - 0.20$	0.82	$1.83 \cdot 10^{-9}$	16.53	0.9091
	25	$y = -1.99 \cdot 10^{-9}x$	1.00	$1.99 \cdot 10^{-9}$	15.85	0.9422
	35	$y = -1.80 \cdot 10^{-9}x + 0.03$	1.03	$1.80 \cdot 10^{-9}$	16.67	0.9216
SG-G2.5	15	$y = -2.15 \cdot 10^{-9}x + 0.04$	1.04	$2.15 \cdot 10^{-9}$	15.25	0.9452
	25	$y = -2.20 \cdot 10^{-9}x + 0.20$	1.22	$2.20 \cdot 10^{-9}$	15.08	0.9731
	35	$y = -2.15 \cdot 10^{-9}x + 0.30$	1.35	$2.15 \cdot 10^{-9}$	15.25	0.9275

Table 5
Thermodynamic parameters for the adsorption

Adsorbent	T (°C)	ΔG (kJ·mol^{-1})	ΔH (kJ·mol^{-1})	ΔS (J·mol^{-1}·K^{-1})
SG-G0.5	15	–20.58	8.98	102.10
	25	–21.12		
	35	–22.65		
SG-G1.5	15	–22.46	10.88	115.05
	25	–22.97		
	35	–24.79		
SG-G2.5	15	–20.79	24.72	157.07
	25	–21.52		
	35	–23.97		

cating the adsorption of Fe(III) onto SG-G0.5, SG-G1.5, and SG-G2.5 is spontaneous. ΔG value decreases with the increase of temperature, implying the adsorption favors high temperature. The values of ΔH are positive, suggests the endothermic nature of the adsorption, which is consistent with the results of adsorption isotherm.

The positive values of ΔS demonstrate entropy increased during the adsorption, which can be attributed to the release of ethanol molecules from the solvation Fe(III) ions during the adsorption. Before adsorption occurs, the Fe(III) ion exists in the form of alcoholate form with ethanol molecules surrounding in the periphery. During the adsorption process, the ethanol molecules would be substituted by the functional groups of PAMAM dendrimers, leading to the release of ethanol molecules and entropy increase [7].

3.5. Effect of adsorbent dosage on adsorption

The effect of adsorbent dosage on the adsorption is presented in Fig. 5, it can be seen the removal rate increases with the increase of adsorbent dosage, while the adsorption capacity displays an inverse trend. Take SG-G2.5 for example, the removal rate increases from 43 % to 95 % with the adsorbent dosage increases from 10 to 60 mg, whereas the adsorption capacity decreases from 0.65 to 0.26 mmol·g^{-1}. The increase of removal rate can be ascribed to the increase of active binding sites with the increase of adsorbent dosage, which can bind more metal ions and enhance the removal rate. However, the ratio of Fe(III)/binding site decreases
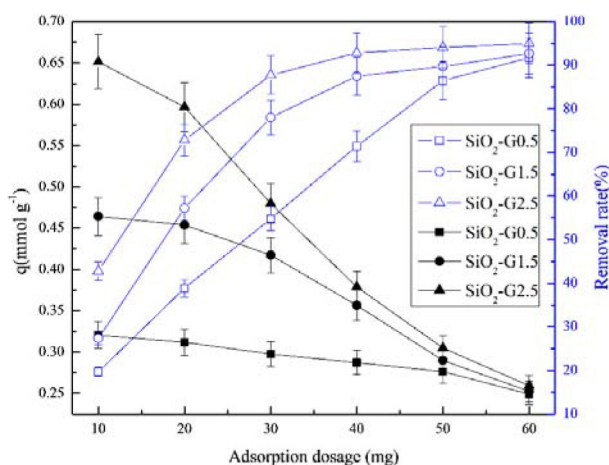
Fig. 5. Effect of adsorbent dosage on the adsorption for Fe(III).

with the increase of adsorbent dosage, leading to the lack of Fe(III) for the binding site, and hence there is a decrease in the adsorption [49].

3.6. Regeneration property

The regeneration property of SG-G0.5, SG-G1.5, and SG-G2.5 was tested by employing 5% thiourea-0.5 mol·L^{-1} HNO$_3$ as eluent and the results are shown in Fig. 6. It was found that SG-G0.5~SG-G2.5 all exhibit excellent regeneration property and can reserve at least 90% adsorption rate after three cycles of adsorption-desorption, indicating these adsorbents can be used as cost-effective adsorbent for the removal of Fe(III) from ethanol.

3.7 Adsorption mechanism

The FTIR spectra of SG-G0.5, SG-G1.5, and SG-G2.5 before and after adsorption are shown in Fig. 7. For
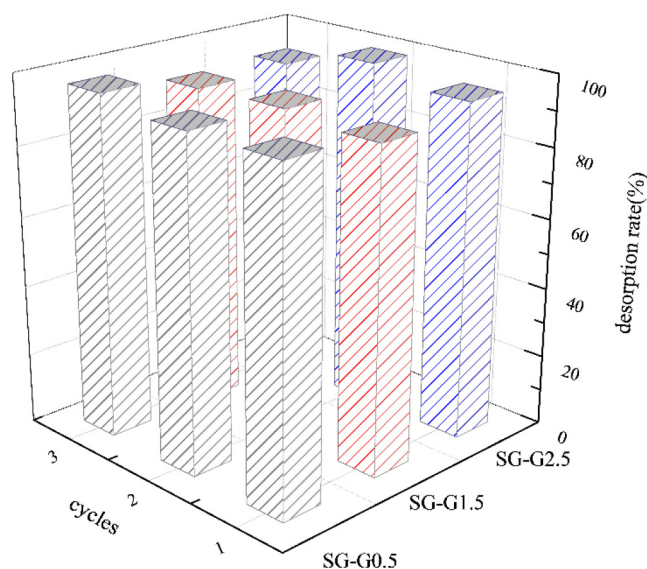

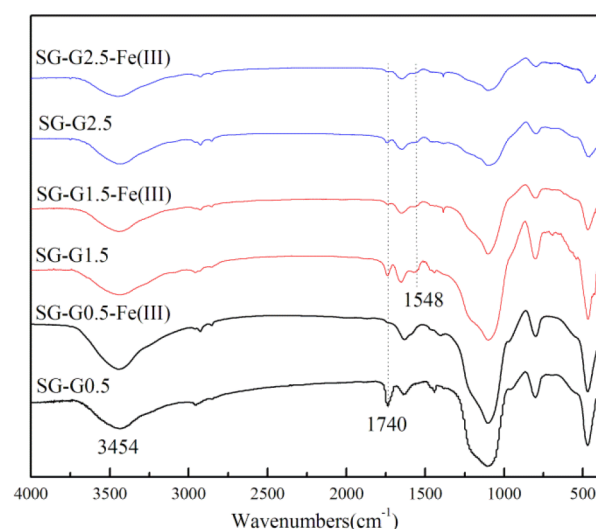Fig. 6. The regeneration property of the adsorbents.

Fig. 7. The FTIR spectra of adsorbents before and after adsorption for Fe(III).

SG-G0.5, SG-G1.5, and SG-G2.5, the absorption band around 3454 cm^{-1} is attributed to the stretching vibration of the −OH group, and the characteristic adsorption peak of -COOCH$_3$ appears at 1740 cm^{-1}. For SG-G1.5 and SG-G2.5, the bands at 1548 cm^{-1} belong to the stretching vibration N-H group. After adsorption, the characteristic absorption peak of ester group is disappeared completely, and that of N-H bond is also became weaker, which indicate the participation of ester and amide group during the adsorption process.

In order to further reveal the adsorption mechanism, DFT calculation was conducted and the optimized geometry of the complexes as well as the bond distance is presented in Fig. 8. It can be seen that G0.5 mainly coordinates with Fe(III) with two mode. One is to coordinate with Fe(III) by two carbonyl oxygen atom (G0.5-Fe(III)-1) and the bond distance of Fe-O is 1.90 Å, another is to bind Fe(III) with two carbonyl oxygen and two secondary amine nitrogen atoms to form tetra-coordinated complex (G0.5-Fe(III)-2). The bond distances of Fe-O are 1.94 and 1.95 Å, while those of Fe-N are 2.01 and 2.02 Å for G0.5-Fe(III)-2, respectively. The binding energy of G0.5-Fe(III)-1 and G0.5-Fe(III)-2 is
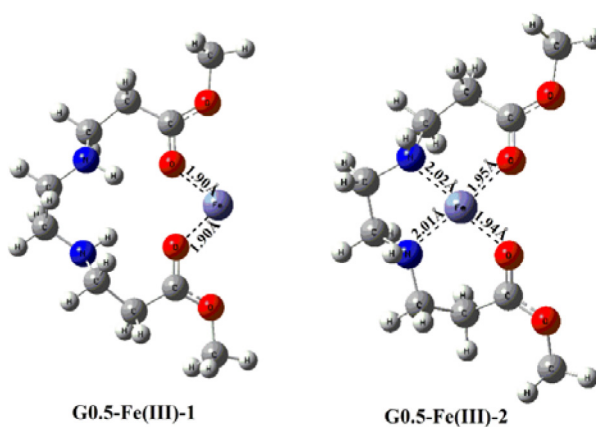

Fig. 8. The optimized geometry of the complexes.

–794.04 and –822.89 kcal/mol, indicating the interaction of Fe(III) by forming tetra-coordinated complex dominates the adsorption.

NBO analysis was employed to evaluate the charge transfer and the magnitude of the interaction between donor and acceptor atoms [7,50]. The NBO partial charges of Fe(III) in the complexes of G0.5-Fe(III)-1 and G0.5-Fe(III)-2 are 1.44 and 1.51, suggesting the existence of charge transfer from ligand to Fe(III) during the adsorption. The stabilization energy $E(2)$ based on NBO analysis was employed to estimate the interactions between functional group (donor) and Fe(III) (acceptor). For G0.5-Fe(III)-1, the interaction between ligand and Fe(III) dominates by the σ donation of oxygen lone pair electrons to the empty orbital of Fe(III) ((LP(O)→LP*(Fe)), and the stabilization energies $E(2)$ are 18.70 kcal/mol. Similar to G0.5-Fe(III)-1, the σ donation of LP(O)→LP*(Fe) with $E(2)$ energies of 2.20 and 2.13 also contributes to the coordination of G0.5-Fe(III)-1. Moreover, the electron transfer from lone pair electrons of oxygen to the antibond of N-Fe ((LP(O)→ BD*(N-Fe)) plays more important part in the adsorption, and the $E(2)$ energies are 39.18 and 37.07 kcal/mol. The results indicate the adsorption of silica-gel supported ester-terminated PAMAM dendrimers mainly involves the interaction of carbonyl oxygen and a mine nitrogen groups with Fe(III).

4. Conclusions

The adsorption property of SG-G0.5, SG-G1.5, and SG-G2.5 for Fe(III) in ethanol were investigated systematically by considering the effects of dendrimer generation, contact time, temperature, initial Fe(III) concentration, and adsorbent dosage on the adsorption. The adsorption capacity increases with the increasing of dendrimer generation by following the order of SG-G2.5 > SG-G1.5 > SG-G0.5. Adsorption kinetic can be well fitted by pseudo-second-order model and is controlled by film diffusion process. Adsorption isotherm demonstrates the adsorption favors high temperature and initial Fe(III) concentration. The adsorption isotherm follows Langmuir model and carries out by monolayer chemical ion-exchange mechanism. Thermodynamic parameters imply the adsorption process is a spontaneous, endothermic and randomness increased process. The regeneration property shows the adsorbents exhibit good reusability and maintain excellent adsorption capacity after three cycles of adsorption-desorption. Adsorption mechanism indicate the interaction of carbonyl oxygen and a mine nitrogen groups with Fe(III) mainly dominate the adsorption process.

Acknowledgements

References

[1] S. Davis, K. Caldeira, H. Matthews, Future CO_2 emissions and climate change from existing energy infrastructure, Science, 329 (2010) 1330–1333.

[2] B. Booth, N. Bellouin, Climate change black carbon and atmospheric feedbacks, Nature, 519 (2015) 167–168.

[3] H. Schaefer, S. Fletcher, C. Veidt, K. Lassey, G. Brailsford, T. Bromley, E. Dlugokencky, S. Michel, J. Miller, I. Levin, D. Lowe, R. Martin, B. Vaughn, J. White, A 21st-century shift from fossil-fuel to biogenic methane emissions indicated by (CH_4)-C-13, Science, 352 (2016) 80–84.

[4] D. Hsu, D. Inman, G. Heath, E. Wolfrum, M. Mann, A. Aden, Life cycle environmental impacts of selected US ethanol production and use pathways in 2022, Environ. Sci. Technol., 44 (2010) 5289–5297.

[5] S. Li, N. Zhang, X. Xie, R. Luque, Y. Xu, Stress-transfer-induced in situ formation of ultra thin nickel phosphide nanosheets for efficient hydrogen evolution, Angew. Chem. Int. Edit., 57 (2018) 13082–13085.

[6] Y. Xie, Y. Ben-David, L. Shimon, D. Milstein, Highly efficient process for production of biofuel from ethanol catalyzed by ruthenium pincer complexes, J. Am. Chem. Soc., 138 (2016) 9077–9080.

[7] X. Song, Y. Niu, P. Zhang, C. Zhang, Z. Zhang, Y. Zhu, R. Qu, Removal of Co(II) from fuel ethanol by silica-gel supported PAMAM dendrimers: Combined experimental and theoretical study, Fuel, 199 (2017) 91–101.

[8] C. Leite, A. de Jesus, M. Potes, M. Vieira, D. Samios, M. Silva, Direct determination of Cd, Co, Cu, Fe, Mn, Na, Ni, Pb, and Zn in ethanol fuel by high-resolution continuum source flame atomic absorption spectrometry, Energy Fuel, 29 (2015) 7358–7363.

[9] A. Prado, I. Pescara, S. Evangelista, M. Holanda, R. Andrade, P. Suarez, L. Zara, Adsorption and preconcentration of divalent metal ions in fossil fuels and biofuels: Gasoline, diesel, biodiesel, diesel-like and ethanol by using chitosan micro spheres and thermodynamic approach, Talanta, 84 (2011) 759–765.

[10] X. Song, Y. Niu, Z. Qiu, Z. Zhang, Y. Zhou, J. Zhao, H. Chen, Adsorption of Hg(II) and Ag(I) from fuel ethanol by silica gel supported sulfur-containing PAMAM dendrimers: Kinetics, equilibrium and thermodynamics, Fuel, 206 (2017) 80–88.

[11] C. Maroneze, H. Magosso, A. Panteleimonov, Y. Kholin, Y. Gushikem, Surface functionalization of SBA-15 and a nonordered mesoporous silica with a 1,4-diazabicyclo 2.2.2 octane derivative: Study of $CuCl_2$ adsorption from ethanol solution, J. Colloid Interf. Sci., 356 (2011) 248–256.

[12] E. Vieira, I. Soares, G. Pires, R. Ramos, D. do Carmo, N. Dias Filho, Study on determination and removal of metallic ions from aqueous and alcoholic solutions using a new POSS adsorbent, Chem. Eng. J., 264 (2015) 77–88.

[13] L. Ma, S. Islam, C. Xiao, J. Zhao, H. Liu, M. Yuan, G. Sun, H. Li, S. Ma, M.G. Kanatzidis, Rapid simultaneous removal of toxic anions $[HSeO_3]^-$, $[SeO_3]^{2-}$, and $[SeO_4]^{2-}$, and metals Hg^{2+}, Cu^{2+}, and Cd^{2+} by MoS_4^{2-} intercalated layered double hydroxide, J. Am. Chem. Soc., 139 (2017) 12745–12757.

[14] Z. Zhang, X. Liu, K. Wang, Y. Niu, H. Chen, L. Bai, Z. Xue. Removal of Ag(I) from aqueous solution by thiourea-functionalized silica gel: Experimental and theoretical study, Desal. Water Treat., 151 (2019) 307–314.

[15] B. Chen, H. Zhao, S. Chen, F. Long, B. Huang, B. Yang, X. Pan, A magnetically recyclable chitosan composite adsorbent functionalized with EDTA for simultaneous capture of anionic dye and heavy metals in complex wastewater, Chem. Eng. J., 356 (2019) 69–80.

[16] L. Dong, L. Hou, Z. Wang, P. Gu, G. Chen, R. Jiang, A new function of spent activated carbon in BAC process: Removing heavy metals by ion exchange mechanism, J. Hazard. Mater., 359 (2018) 76–84.

[17] D. Pakulski, W. Czepa, S. Witomska, A. Aliprandi, P. Pawluc, V. Patroniak, A. Ciesielski, P. Samori, Graphene oxide-branched polyethylenimine foams for efficient removal of toxic cations from water, J. Mater. Chem. A., 6 (2018) 9384–9390.

[18] S. Wang, Y. Peng, Natural zeolites as effective adsorbents in water and wastewater treatment, Chem. Eng. J., 156 (2010) 11–24.

[19] Y. Niu, R. Qu, H. Chen, L. Mu, X. Liu, T. Wang, Y. Zhang, C. Sun, Synthesis of silica gel supported salicylaldehyde modified PAMAM dendrimers for the effective removal of Hg(II) from aqueous solution, J. Hazard. Mater., 278 (2014) 267–278.

[20] T. Fu, Y. Niu, Y. Zhou, K. Wang, Q. Mu, R. Qu, H. Chen, B. Yuan, H. Yang, Adsorption of Mn(II) from aqueous solution by silica-gel supported polyamidoamine dendrimers: Experimental and DFT study, J. Taiwan Inst. Chem. E., 97 (2019) 189–199.

[21] J. Aguado, J. Arsuaga, A. Arencibia, M. Lindo, V. Gascon, Aqueous heavy metals removal by adsorption on a mine-functionalized mesoporous silica, J. Hazard. Mater., 163 (2009) 213–221.

[22] E. Da'na, Adsorption of heavy metals on functionalized-mesoporous silica: A review, Micropor. Mesopor. Mat., 247 (2017) 145–157.

[23] Y. Niu, H. Liu, R. Qu, S. Liang, H. Chen, C. Sun, Y. Cui, Preparation and characterization of thiourea-containing silica gel hybrid materials for Hg(II) adsorption, Ind. Eng. Chem. Res., 54 (2015) 1656–1664.

[24] J. Cross, M. Lauz, P. Badger, S. Petoud, Polymetallic lanthanide complexes with PAMAM-naphthalimide dendritic ligands: Luminescent lanthanide complexes formed in solution, J. Am. Chem. Soc., 126 (2004) 16278–16279.

[25] Y. Jiang, Q. Gao, H. Yu, Y. Chen, F. Deng, Intensively competitive adsorption for heavy metal ions by PAMAM-SBA-15 and EDTA-PAMAM-SBA-15 inorganic-organic hybrid materials, Micropor. Mesopor. Mat., 103 (2007) 316–324.

[26] P. Zhang, Y. Niu, W. Qiao, Z. Xue, L. Bai, H. Chen, Experimental and DFT investigation on the adsorption mechanism of silica gel supported sulfur-capped PAMAM dendrimers for Ag(I), J. Mol. Liq., 263 (2018) 390–398.

[27] M. Sajid, M.N. Ihsanullah, N. Baig, A. Osman, Removal of heavy metals and organic pollutants from water using dendritic polymers based adsorbents: A critical review, Sep. Purif. Technol., 191 (2018) 400–423.

[28] Y. Niu, R. Qu, C. Sun, C. Wang, H. Chen, C. Ji, Y. Zhang, X. Shao, F. Bu, Adsorption of Pb(II) from aqueous solution by silica-gel supported hyper branched polyamidoamine dendrimers, J. Hazard. Mater., 244–245 (2013) 276–286.

[29] X. Wu, P. Liu, Q. Pu, Q. Sun, Z. Su, Preparation of dendrimer-like polyamidoamine immobilized silica gel and its application to online preconcentration and separation palladium prior to FAAS determination, Talanta, 62 (2004) 918–923.

[30] X. Wu, L. Luo, Z. Chen, K. Liang, Syntheses, characterization and adsorption properties for Pb²⁺ of silica-gel functionalized by dendrimer-like polyamidoamine and 5-sulfosalicylic acid, Appl. Surf. Sci., 364 (2016) 86–95.

[31] R. Qu, C. Sun, F. Ma, Z. Cui, Y. Zhang, X. Sun, C. Ji, C. Wang, P. Yin, Adsorption kinetics and equilibrium of copper from ethanol fuel on silica-gel functionalized with amino-terminated dendrimer-like polyamidoamine polymers, Fuel, 92 (2012) 204–210.

[32] M.J. Frisch, TGW, G.E. Scuseria HBS, M.A. Robb, J.R. Cheeseman, JAJ Montgomery, T. Vreven, K.N. Kudin, J.C. Burant, J.M. Millam, S.S. Iyengar, J. Tomasi, V. Barone, B. Mennucci, M . Cossi, G. Scalmani, N. Rega, G.A. Petersson, H. Nakatsuji, M. Hada, M. Ehara, K. Toyota, R. Fukuda, J. Hasegawa, M. Ishida, T. Nakajima, Y. Honda, O. Kitao, H. Nakai, M. Klene, X. Li, J.E. Knox, H.P. Hratchian, J.B. Cross, C.J. Jaramillo, R. Gomperts, R.E. Stratmann, O. Yazyev, A.J. Austin, R. Cammi, C. Pomelli, J.W. Ochterski, P.Y. Ayala, K. Morokuma, G.A. Voth, P. Salvador, J.J. Dannenberg, V.G. Zakrzewski, S Dapprich, A.D. Daniels, M.C. Strain, O. Farkas, D.K. Malick, A.D. Rabuck, K. Raghavachari, J.B. Foresman, J.V. Ortiz, Q Cui, A.G. Baboul, S. Clifford, J. Cioslowski, B.B. Stefanov, G. Liu, A. Liashenko, P. Piskorz, I. Komaromi, R.L. Martin, D.J. Fox, T. Keith, M.A. Al-Laham, C.Y. Peng, A. Nanayakkara, M. Challacombe, PMW Gill, B. Johnson, W. Chen, M.W. Wong, C. Gonzalez, J.A. Pople Gaussian 03, Revision C.02, Gaussian, Inc.: Wallingford, CT, 2004.

[33] Z. Zhang, Y. Niu, H. Chen, Z. Yang, L. Bai, Z. Xue, H. Yang, Feasible one-pot sequential synthesis of aminopyridine functionalized magnetic Fe₃O₄ hybrids for robust capture of aqueous Hg(II) and Ag(I), ACS Sustain. Chem. Eng., 7 (2019) 7324–7337.

[34] D. Setyono, S. Valiyaveettil, Functionalized paper-A readily accessible adsorbent for removal of dissolved heavy metal salts and nanoparticles from water, J. Hazard. Mater., 302 (2016) 120–128.

[35] H. Li, Y. Niu, Z. Xue, Q. Mu, K. Wang, R. Qu, H. Chen, L. Bai, H. Yang, D. Wei, Adsorption property and mechanism of PAMAM dendrimer/silica gel hybrids for Fe(III) and Ag(I) from N,N-dimethylformamide, J. Mol. Liq., 273 (2019) 305–313.

[36] O. Siig, K. Kepp, Iron(II) and iron(III) spin crossover: Toward an optimal density functional, J. Phys. Chem. A., 122 (2018) 4208–4217.

[37] J. Zhao, Y. Niu, B. Ren, H. Chen, S. Zhang, J. Jin, Y. Zhang, Synthesis of Schiff base functionalized super paramagnetic Fe₃O₄ composites for effective removal of Pb(II) and Cd(II) from aqueous solution, Chem. Eng. J., 347 (2018) 574–584.

[38] Y. Ho, G. McKay, Kinetic models for the sorption of dye from aqueous solution by wood, Process Saf. Environ., 76 (1998) 183–191.

[39] Y. Ho, G. McKay, Sorption of dye from aqueous solution by peat, Chem. Eng. J., 70 (1998) 115–124.

[40] Z. Qiu, Y. Niu, T. Fu, K. Wang, Q. Mu, F. Wang, Removal of Ni(II) from fuel ethanol by PAMAM dendrimers/silica hybrid materials: Combined experimental and theoretical study, Chem. Eng. Res. Des., 144 (2019) 174–184.

[41] G. Boyd, A. Adamson, L. Myers, The exchange adsorption of ions from aqueous solutions by organic zeolites. II. Kinetics1, J. Am. Chem. Soc., 69 (1947) 2836–2848.

[42] D. Reichenberg, Properties of ion-exchange pesins in relation to their structure. III. Kinetics of exchange, J. Am. Chem. Soc., 75 (1953) 589–597.

[43] A. Ramesh, H. Hasegawa, W. Sugimoto, T. Maki, K. Ueda, Adsorption of gold(III), platinum(IV) and palladium(II) onto glycine modified cross linked chitosan resin, Bioresource Technol., 99 (2008) 3801–3809.

[44] Z. Reddad, C. Gerente, Y. Andres, P. Le Cloirec, Adsorption of several metal ions onto a low-cost biosorbent: Kinetic and equilibrium studies, Environ. Sci. Technol., 36 (2002) 2067–2073.

[45] D. Mohan, K. Singh, Single- and multi-component adsorption of cadmium and zinc using activated carbon derived from bagasse-an agricultural waste, Water Res., 36 (2002) 2304–2318.

[46] A. Ofomaja, Equilibrium studies of copper ion adsorption onto palm kernel fibre, J. Environ. Manage., 91 (2010) 1491–1499.

[47] Y. Niu, R. Qu, X. Liu, L. Mu, B. Bu, Y. Sun, Hou Chen, Y. Meng, L. Meng, L. Cheng, Thiol-functionalized polysilsesquioxane as efficient adsorbent for adsorption of Hg(II) and Mn(II) from aqueous solution, Mater. Res. Bull., 52 (2014) 134–142.

[48] F. Ma, N. Zhang, X. Wei, J. Yang, Y. Wang, Z. Zhou, Blend-electrospun poly(vinylidene fluoride)/polydopamine membranes: self-polymerization of dopamine and the excellent adsorption/separation abilities, J. Mater. Chem. A., 5 (2017) 14430–14443.

[49] K. Jung, S. Lee, Y. Lee, Hydrothermal synthesis of hierarchically structured birnessite-type MnO₂/biochar composites for the adsorptive removal of Cu(II) from aqueous media, Bioresource Technol., 260 (2018) 204–212.

[50] M. Costa, L. Prates, L. Baptista, M. Cruz, I. Ferreira, Interaction of polyelectrolyte complex between sodium alginate and chitosan dimers with a single glyphosate molecule: A DFT and NBO study, Carbohyd. Polym., 198 (2018) 51–60.

Supplementary information

2.1. Adsorption properties for Fe(III)

2.1.1. Kinetic adsorption

Adsorption kinetic was carried out by placing a series of 25 mg adsorbent to the flasks that containing 20 mL 0.001 mol·L^{-1} Fe(III) solution. The flasks were shaken at 25°C and the concentration of Fe(III) was determined at different time intervals. Afterward, the adsorption capacity was calculated.

The pseudo-first-order model, pseudo-second-order kinetic model, and Boyd film diffusion model were fitted with experimental data to reveal the adsorption kinetic mechanism. The linear equation of pseudo-first-order and pseudo-second-order models can be expressed by Eqs. (1) and (2), respectively.

$$In(q_e - q) = In q_e - k_1 t \tag{1}$$

$$\frac{t}{q} = \frac{1}{k_2 q_e^2} + \frac{1}{q_e} t \tag{2}$$

where q and q_e are the adsorption capacity at time t and equilibrium (mmol·g^{-1}); t is the adsorption time (min); k_1 (min^{-1}) and k_2 (g·mmol^{-1}·min^{-1}) represent the pseudo-first-order and pseudo-second-order model rate constant.

Boyd film diffusion model expressed by Eq. (3) is further employed to explore whether film diffusion or intraparticle diffusion is the rate-controlling step.

$$F = 1 - \frac{6}{\pi^2} \sum_{n=1}^{\infty} \frac{1}{n^2} \exp\left[-n^2 Bt\right] \tag{3}$$

where n is an integer which defines the infinite series solution; B is time constant; and F represents the fractional attainment of equilibrium at time t and can be obtained from Eq. (4):

$$F = \frac{q_t}{q_e} \tag{4}$$

where q_t and q_e are adsorption capacity at time t and equilibrium.

The value of B_t can be acquired from the corresponding F value as given by Reichenbery [1]. The linearity of B_t versus t plot can be used to evaluate whether film or intraparticle diffusion is the rate-controlling step of the adsorption. If the fitting plot shows good linearity without passing through the origin, the adsorption is controlled by film diffusion. As an alternative, if the linear plot passes through the origin, intraparticle diffusion would dominate the adsorption.

2.1.2. Isotherm adsorption

About 25 mg adsorbent was added to a series of flasks containing 20 mL Fe(III) solution with different concentration. The mixture was shaken for 12 h at 15°C, 25°C, and 35°C, respectively. Afterward, the concentration was determined and the adsorption capacity was calculated.

Langmuir, Freundlich, and Dubinin-Radushkevich (D-R) models are applied to fit the isotherm data. Langmuir model assumes the adsorption takes place on homogeneous surface via monolayer adsorption, while Freundlich model is applied for the adsorption on heterogeneous surface with non-uniform distribution of energy by multilayer adsorption. The linear forms of the two models can be described by Eqs. (5) and (6):

$$\frac{C_e}{q_e} = \frac{C_e}{q_m} + \frac{1}{q_m K_L} \tag{5}$$

$$In\,q_e = In\,K_F + \frac{In C_e}{n} \tag{6}$$

where q_e and q_m resemble the equilibrium adsorption amount and maximum adsorption amount (mmol·g^{-1}), C_e denotes the equilibrium concentration (mmol·mL^{-1}), K_L represents the Langmuir constants (mL·mmol^{-1}), K_F is the Freundlich constants (mmol·g^{-1}), and n is the constant (dimensionless).

D-R model is also utilized to estimate whether the adsorption proceeds chemically or physically. The linear form of D-R model is described as Eq. (7):

$$In\,q_e = In\,q_m - \beta \varepsilon^2 \tag{7}$$

where q_e and q_m are the equilibrium adsorption amount and maximum adsorption amount (mmol·g^{-1}); β is mean free energy activity coefficient (mol^2·J^{-2}); ε is the polanyi potential energy (kJ^2·mol^{-2}) that can be calculated from Eq. (8):

$$\varepsilon = RT\,In\left(1 + \frac{1}{C_e}\right) \tag{8}$$

The mean free energy can be achieved by the β value according to Eq. (9):

$$E = \frac{1}{\sqrt{2\beta}} \tag{9}$$

The E value can be utilized to estimate the nature of the adsorption process. When it is higher than 8 KJ·mol^{-1}, the adsorption would proceed by chemical ion-exchange mechanism. Otherwise, if it bellows 8 KJ·mol^{-1}, the adsorption is physical in nature [2].

References

[1] D. Reichenberg, Properties of ion-exchange pesins in relation to their structure. III. Kinetics of exchange, J. Am. Chem. Soc., 75 (1953) 589–597.

[2] A. Ofomaja, Equilibrium studies of copper ion adsorption onto palm kernel fibre, J. Environ. Manage., 91 (2010) 1491–1499.